A theoretical model for intermediate debonding of RC beams strengthened in bending by FRP

C. Faella
Dipartimento di Ingegneria Civile, Università di Salerno, Italy

E. Martinelli
Dipartimento di Ingegneria Civile, Università di Salerno, Italy

E. Nigro
Dipartimento di Analisi e Progettazione Strutturale, Università di Napoli "Federico II", Italy

ABSTRACT: In the present paper, a mechanical model accounting for the interface stress-slip relationship is presented with the aim of simulating the behavior of RC beams strengthened by externally bonded FRP systems. Finite element implementation and validation of such a model will be outlined with the aim of pointing out the capability of the proposed procedure of reproducing both end and intermediate debonding phenomena which often affect the overall behavior of FRP-strengthened beams. Behavioral observations will be pointed out for emphasizing the role of the key parameters controlling premature (fracture energy, steel yielding strain, reinforcement amount, etc.) failure due to intermediate debonding.

1 INTRODUCTION

Improving flexural strength in RC members by bonding FRP laminates at their soffit is one of the most common strengthening techniques which can face either a rebar section reduction due to steel corrosion or an increase of actions applied upon the member. Nevertheless the possible premature failure due to debonding between adhesive layer and concrete, which can occur at the beam end (end debonding) or in the cracked zone (intermediate debonding), is one of the failure modes to be prevented.
In the last years huge research efforts have been carried out for understanding the behavior of reinforced concrete beams strengthened by externally bonded FRP. Many of these studies are focused on the formulation of mechanical models, either analytical or numerical in their possible implementation, able to simulate the complex stress and strain distribution throughout the FRP-to-concrete adhesive interface.
Different contributions about this topic have been summarized and compared by Chen & Teng (2001). A simplified model for evaluating interface stresses in FRP (or even steel) strengthened beams has been proposed by Roberts (1988); simplified equations for evaluating shear and normal stresses throughout the FRP-to-concrete interface have been provided by assuming linear elastic behavior of the adhesive interface. Similar relationships, even obtained under simplified hypotheses for interface behavior, have been also provided by Malek et Al. (1996).
The above mentioned papers mainly deal with interface stress distribution in the elastic range, which is an aspect mainly relevant in service conditions. Premature loss of bonding between FRP and concrete can only be simulated by considering a suitable non-linear relationship between interface stresses and strains. Holzenkaempfer (1994) proposed a bi-linear relationship between shear stresses and interface slips; based on such model, Taljsten (1997) determined the expression of the ultimate bearing capacity of FRP-to-concrete joints. Further studies have been devoted to end and intermediate debonding, but nowadays definitive solutions have not yet been reached. Nevertheless, several proposals for quantifying the maximum axial strain developed in FRP at debonding have been derived from simplified mechanical models and calibrated making use of the experimental results available in the scientific literature. Some of the findings of these studies have been also utilized in the following Code of Standards issued in various countries:
- fib bulletin 14 (2001) in Europe;
- ACI 440 (2002) in the United States;
- JSCE Recommendations (2001) in Japan;
- Italian Code CNR DT 200 (2004).

A mechanical model considering non-linear stress-strain relationships for concrete, steel and FRP-to-concrete interface has been already presented by the authors (Faella et Al., 2006), with the aim of simulating the behavior of RC beams strengthened by externally bonded FRP plates. The model, whose hypotheses will be shortly summarized in the following, has been also validated in the same paper by considering almost thirty experimental results obtained by different authors; the experimental-to-numerical comparison pointed out that the model is able to capture both the overall behavior and the

failure load. The axial strain developed in FRP at U.L.S. is one of the key parameters to be observed in the analyses; in fact, debonding can occur at the FRP-to-concrete interface reducing the beam bearing capacity with respect to the one obtained for FRP tearing-rupture. The mentioned numerical model is able to assess the FRP effective axial strain at debonding, allowing to point out the key parameters which control debonding failure.

2 THE THEORETICAL MODEL

In the present section an analytical model is presented for simulating the behavior of FRP-strengthened RC beams. Moreover, the formulation of a finite element is presented and a secant procedure for non-linear analysis is also described.

2.1 *Analytical formulation within the linear range*

A theoretical model can be formulated for simulating the mechanical behavior of RC beams externally strengthened by means of FRP materials. The following assumptions are made:

- the RC beam behaves according to the Bernoulli theory, while FRP plate flexural stiffness is neglected and only axial forces are considered;
- the interaction between the two members is realized through a continuous, linear behaving and thicknessless medium;
- equal transverse displacements, i.e. deflections, occur in the connected members.

The partial interaction between beam and FRP results in an interface slip s which can be expressed as follows if the above hypotheses apply:

$$\begin{aligned} s &= u_{f,sup} - u_{c,inf} = \\ &= u_f - \varphi \cdot y_{f,sup} - \left(u_c + \varphi \cdot y_{c,inf}\right) = u_f - u_c - \varphi \cdot d \end{aligned} \quad (1)$$

with the symbols reported in Figure 1; in particular d is the distance between RC beam and FRP plate centroids. However, assuming the Bernoulli hypothesis for the RC beam, the following equivalence between the external bending moment M and the forces represented in Figure 1 can be stated:

$$M = \chi \cdot EI_c + F \cdot d \quad (2)$$

where χ is the curvature and EI_c is the flexural stiffness of unstrengthened RC beam cross section.
The longitudinal shear force per unit length F' depends linearly on the interface slip s:

$$F' = k \cdot s = k_a b_f \cdot s \quad (3)$$

k being the stiffness constant characterizing shear connection; it can be obtained by multiplying the adhesive slip modulus (namely, transverse stiffness) k_a and the width b_f of the adhesive layer.

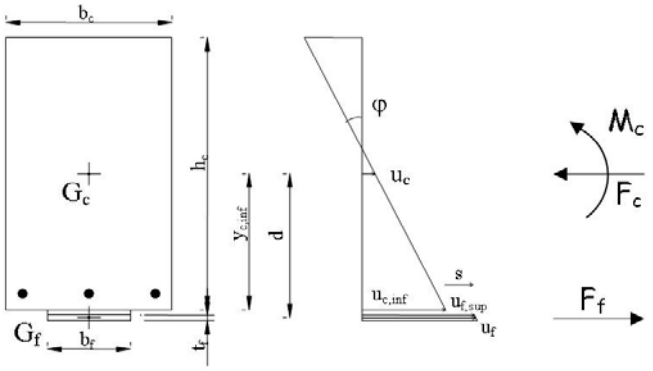

Figure 1. Transverse section of FRP-strengthened RC beam.

Using the compatibility equation (1), the equilibrium equation (2) and the interface relationship (3), the following second-order differential equation in terms of curvature may be obtained:

$$\chi'' - \alpha^2 \chi = -\alpha^2 \frac{M}{EI_{full}} - \frac{q}{EI_c} \quad (4)$$

where EI_{full} represents the flexural stiffness of the overall cross-section when no interface slips occur and can be defined as follows if the above mentioned hypotheses apply:

$$EI_{full} = EI_c + \frac{E_f A_f \cdot EA_c}{E_f A_f + EA_c} d^2 = EI_c + EA^* d^2, \quad (5)$$

the term α in equation (4) is defined as follows:

$$\alpha^2 = \frac{k}{EA^*} \cdot \frac{EI_{full}}{EI_c}. \quad (6)$$

The equations briefly outlined above could even be obtained by simplifying the one formulated within the well-known Newmark theory, widely utilized for steel-concrete composite beams (Faella et Al., 2002), and neglecting the flexural stiffness of the bottom element connected to RC beam.

2.2 *Outlines of the finite element formulation within the mechanically non-linear range*

A finite element can be formulated (among the other possible choices) implementing the exact solution of the structural problem for carrying out linear analyses of RC beams externally strengthened by FRP plates (Faella et Al., 2006). According to the mentioned approach, a formally "force based" finite element can be derived by directly solving equation (4) in order to obtain the various terms of the flexibility matrix **D** and the vector $\boldsymbol{\delta}_0$ of nodal displacements due to distributed loads. The usual relationship of flexibility-based finite elements can be obtained for the simply supported FRP-strengthened beam:

$$\boldsymbol{\delta} = \mathbf{D}\mathbf{X} + \boldsymbol{\delta}_0 \ , \quad (7)$$

X and $\boldsymbol{\delta}$ being the vectors of nodal forces and displacements, respectively, whose four components are represented in Figure 2.

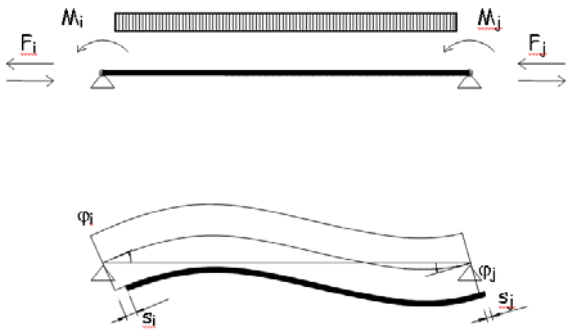

Figure 2. Nodal force and displacement components: simply supported-beam for force based element.

The usual displacement-based relationship which relates nodal forces and displacement for the unrestrained FRP-strengthened beam (Figure 3) can be obtained by inverting the flexibility matrix and completing it with nodal shear forces as explained in the mentioned paper (Faella et Al, 2002). The usual relationship between nodal force vectors **Q**, $\mathbf{Q}_0$, and nodal displacement vectors **s** (both characterized by the six components represented in Figure 3) can be written by means of the stiffness matrix **K**:

$$\mathbf{Q} = \mathbf{K}\mathbf{s} + \mathbf{Q}_0 \ . \qquad (8)$$

Closed-form expression for both stiffness matrix and equivalent nodal force vector have been proposed in Faella et Al. (2000).

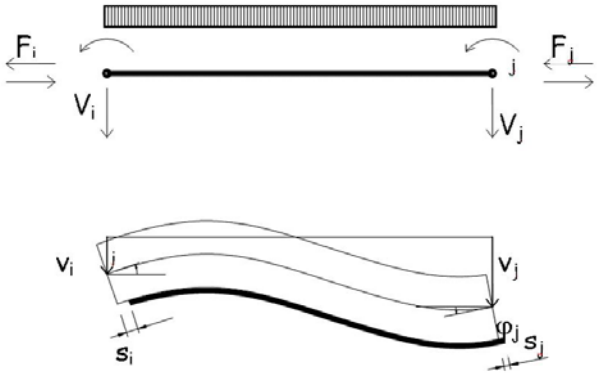

Figure 3. Nodal force and displacement components: unrestrained beam for displacement-based element.

Non linear behavior of the materials of the FRP strengthened RC beams can be easily introduced within the FE procedure. Several non-linear phenomena have to be considered for simulating the premature failure possibly due to FRP-to-concrete debonding which can occur in an intermediate section or at the FRP cut-off section. The first one deals with the overall behavior of concrete in compression and tension; the rational formula proposed by Saenz (1964) is adopted for concrete in compression while a simple linear relationship up to the tensile strength is considered for concrete in tension (Figure 4).
Moreover, intermediate debonding phenomena in FRP-strengthened beams is hugely controlled by rebar yielding; the typical stress-strain relationship for steel rebars is represented in Figure 5 and will be adopted in the numerical analyses. Strain-hardening in steel is actually neglected because strain values in FRP-strengthened beams are usually not so great for strain hardening to be developed in steel rebars.

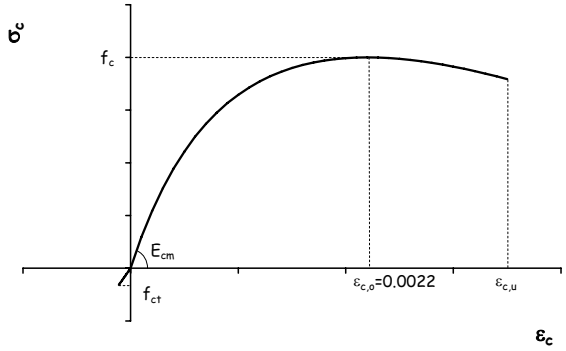

Figure 4. Non-linear stress-strain law for concrete.

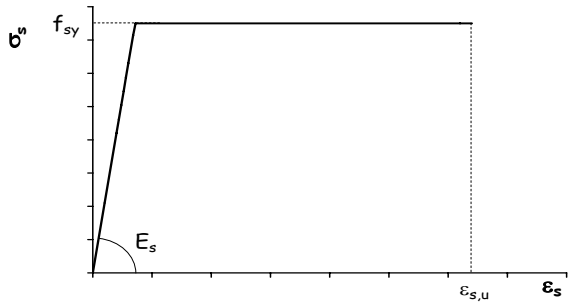

Figure 5. Elastic-perfectly plastic stress-strain law for rebars.

The well-established and widely accepted elastic-brittle stress-strain relationship is assumed for FRP plate (Figure 6). Finally, shear behavior of the adhesive interface connecting FRP laminate or fabric to the soffit of the beam can be described by means of the well-known bi-linear elastic-softening curve (Figure 7) introduced by Holzenkaempfer (1994). The linear branch of the interface law is characterized by the shear stiffness $k_a=k/b_f$ which can be related to the slip modulus k introduced in eq. (2).

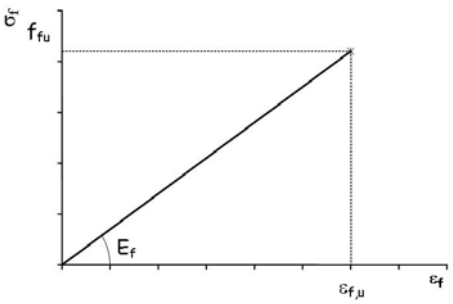

Figure 6. Elastic-brittle stress-strain law for FRP plate.

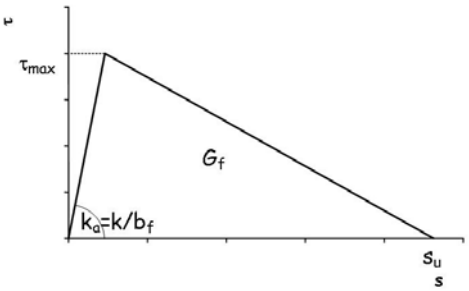

Figure 7. Relationship for FRP-to-Concrete interface

Fiber discretization (Figure 8) is considered for cross section in order to evaluate the secant stiffnesses of reinforced concrete section and the slip modulus of the adhesive interface.

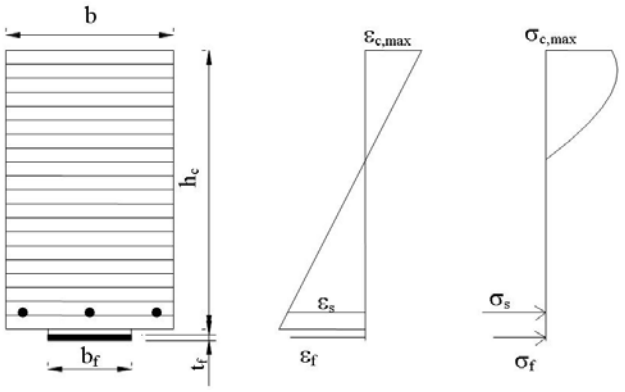

Figure 8. Fiber discretization of the RC beam cross section.

The analysis can be generally pursued until one of the following failure modes is attained:

- concrete crushing, which occurs if the maximum strain value ε_c measured on the concrete fibers at the i-th load step achieves its ultimate value ε_{cu};
- steel rupture, occurring if the steel tensile strain ε_s reaches the corresponding limit value ε_{su};
- FRP plate tearing, if the fiber axial strain ε_f measured in FRP at convergence of the i-th load step achieves the ultimate value ε_{fu};
- FRP debonding, depending on the fact that the maximum interface slip reaches the ultimate value considered in the shear-stress-interface-slip relationship assumed in the analysis.

Further details about the secant procedure implemented for utilizing the proposed Finite Element model along with the relevant results which demonstrate no significant mesh sensitivity of the model can be found in Faella et Al. (2006).

3 DEBONDING FAILURE: BEHAVIORAL OBSERVATIONS

Validation of the proposed procedure can be obtained by comparing numerical and experimental results obtained by one of the various possible campaigns carried out and reported within the scientific literature; the experimental test carried out on the beam A10 in the framework of the campaign reported by Gao et Al. (2004) is considered for validating the numerical procedure. The non-linear stress-strain laws introduced in the previous section are assumed for concrete and steel bars, while elastic-brittle behavior is considered for FRP; the numerical values collected in Table 1 are considered for the corresponding mechanical properties according to data reported by the mentioned authors.

The adhesive interface is modeled by means of the above mentioned bi-linear relationship, whose characteristic parameters are determined according to the fib bulletin 14 – approach 2 proposal reported in the following:

$$\tau_{max} = 0.285 \cdot \sqrt{f_{ck} \cdot f_{ctm}} \quad [\text{MPa}] \tag{9}$$

$$s_u = 0.185 \quad [\text{mm}]. \tag{10}$$

Table 1: Relevant mechanical properties for validation.

Material	Mechanical Property	Numerical Value [MPa]
Concrete	f_{cm}	35.7
	E_{cm}	25000
	f_{ctm}	3.57
Rebar steel	f_{sy}	531
	E_s	200000
FRP	f_{fu}	4200
	E_f	235000
Epoxy resin	f_a	30
	E_a	1000

Slip modulus k_a has been estimated according to the relationship which accounts for both concrete and adhesive shear stiffness G_c and G_a, as pointed out by Faella et Al. (2003) and adopted in CNR DT200 (2004). The value k_a=236.7 N/mm^3 and the value τ_{max} =2.49 MPa have been assumed for the maximum shear stress.

Figure 9 shows the curve relating the value of the total load Q and the corresponding midspan deflection of the beam obtained by means of the proposed procedure. The mentioned figure points out that the numerical model can simulate the overall behavior of the considered FRP-strengthened beam.

Initial stiffness, rebar yielding and premature failure due to intermediate debonding are reproduced with a remarkable precision. Only post-cracking stiffness is underestimated because tension-stiffening effect is completely neglected in the analysis as a result of the elastic-brittle branch considered for concrete in tension (Figure 4). Nevertheless, no refinements have been undertaken herein for taking account of tension stiffening because the issue of concern is the possible intermediate debonding failure which usually occurs after yielding and in condition of completely developed cracks.

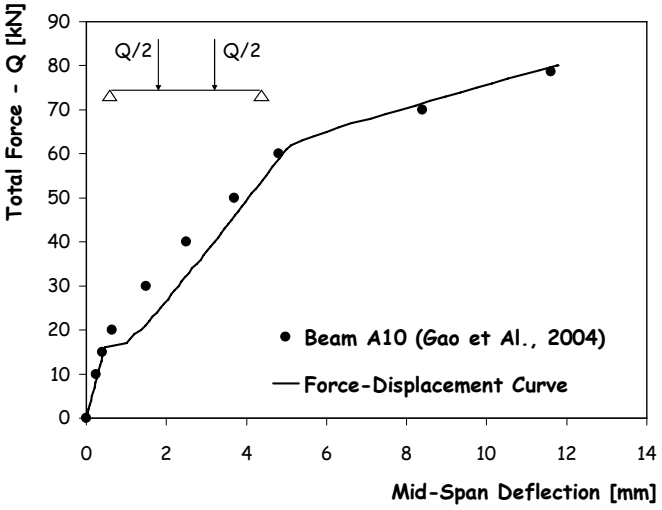

Figure 9. Experimental vs Numerical comparison in terms load-deflection curve (Gao et Al., 2004 – Specimen A10).

Finally, comparing numerical results with respect to only one experimental case could be not sufficient for assessing the accuracy of a numerical procedure for simulating the overall behavior of FRP-

strengthened beams. Consequently, a complete experimental-to-theoretical comparison can be found in Faella et Al. (2006) in terms of force, displacement and FRP axial strain at debonding with respect to the results of more than thirty experimental tests taken by the scientific literature.

4 DEBONDING FAILURE: BEHAVIORAL OBSERVATIONS

In the present section, a short discussion is proposed for showing the two possible debonding failure modes induced by bending which has been observed by various authors and can be reproduced by the proposed model. A simply-supported RC beam is considered in the present section; in a first case it will be considered a complete FRP-strengthening throughout all the beam length, while in a second case it will be interrupted at a distance a=600 mm from the theoretical support point. The beam transverse section is rectangular in shape with a depth h=600 mm and the width b=300 mm; reinforcing steel area at the bottom of the section is A_s=900 mm^2 (0.5% of the transverse section area) and the FRP area is 180 mm^2 (b_f=75 mm), which corresponds to 0.1% of A_c. A value E_f=205 GPa is assumed for FRP Young modulus.

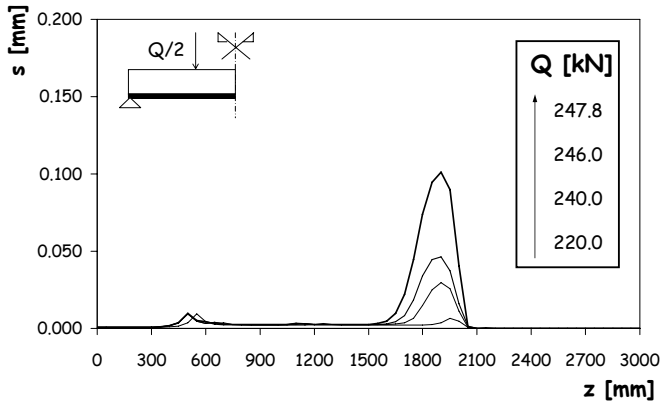

a) interface slips for various load levels up to debonding;

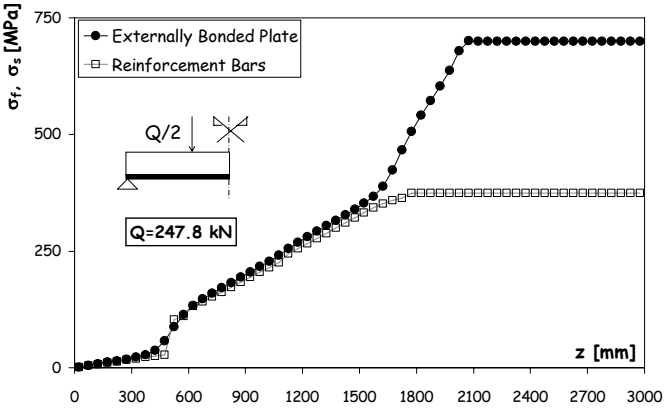

b) axial strains in steel and FRP at debonding ;

Figure 10. Intermediate debonding phenomenon for complete strengthening.

For the first case, Figure 10 shows the interface slip evolution under increasing load levels (Figure 10a) and the axial stress in steel rebars and FRP plate at debonding (Figure 10b). They both deal with the beam characterized by FRP strengthening running throughout all the beam length and show how two peak values can be recognized in interface slips. The first and most relevant one is achieved in correspondence of the steel rebar yielding: it increases sharply at the steel yielding section resulting in intermediate debonding. Such local slip growth is due to the fact that load after yielding is only carried out by FRP plate as one can see in Figure 10b, where a sudden increase in FRP strain slope can be observed starting from the above mentioned section. Another peak in slip value occurs near the support due to flexural cracking whose effects can be also observed in terms of FRP and steel axial stresses: slope changes suddenly in the section where cracking begins at about 500 mm from the theoretical support.

Figure 11 shows the relationship between the applied load Q and the maximum strain $\varepsilon_{f,db}$ developed in FRP for the considered beam pointing out the principal states of stress for concrete, steel and the adhesive interface. Concrete cracking induced by bending results in a sudden transition between the uncracked to the cracked state as already pointed out in the previous section devoted to validation. An almost linear branch is followed up to rebar steel yielding which results in a sharp reduction of bending stiffness.

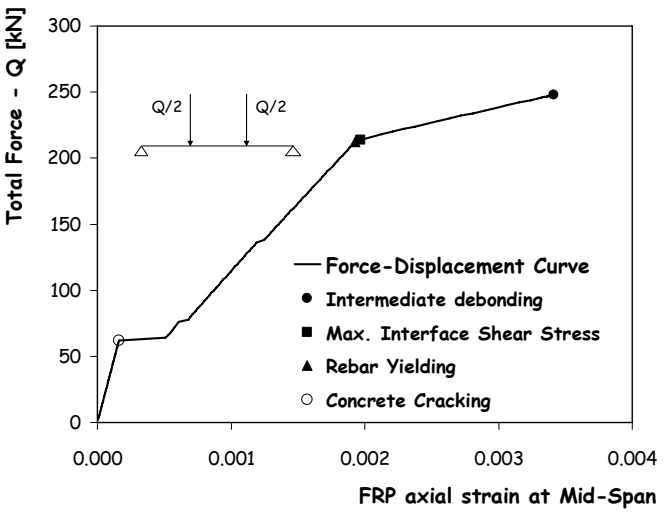

Figure 11. Debonding phenomenon for partial strengthening – Force-FRP strain curve.

Interface shear stresses abruptly increases after yielding as one can see in terms of interface relative displacements in Figure 10a and increments in bending moment can be only carried by FRP. Consequently, after yielding adhesive interface is charged of resisting to a shear stress as great as the total shear force Q/2 and the maximum value of interface shear stress τ_{max} is suddenly achieved after yielding, as one can see in and Figure 11 which directly

shows the increase in axial strain at midspan after the achievement of the maximum interface shear stress τ_{max}. The great part of numerical models available within the scientific literature usually neglects the softening branch of the interface stress-strain law, resulting in underestimating the beam response after the achievement of the maximum interface shear stress and, consequently, a quite significant aspect of its mechanical behavior. As shown in Figure 11, a little increase in terms of bearing capacity can be observed after the achievement of τ_{max}; on the contrary, a significant increase in axial deformation developed in FRP can be observed after reaching τ_{max}. This though limited ductility has been experimentally observed by various authors within the scientific literature as one of the key difference between intermediate and end debonding; both these failure modes are premature in nature with respect to the usual crises due to concrete crushing or steel failure, but the first one is at least less fragile than the second one which occurs after steel yielding.

Continuing about the difference between end and intermediate debonding, Figure 12 deals with the case of incomplete FRP-strengthening. A different peak value can be observed in this case either in terms of slip concentration near the FRP cut-off section (Figure 12a) or in terms of FRP stress whose distribution along the beam interface is characterized by two different slope changes (Figure 12b).

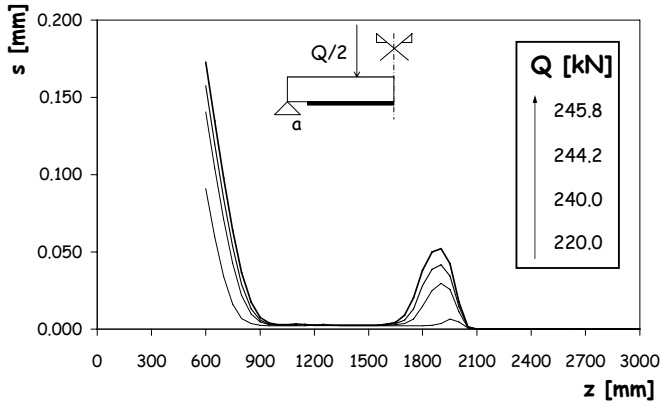

a) interface slips for various load levels up to (end) debonding;

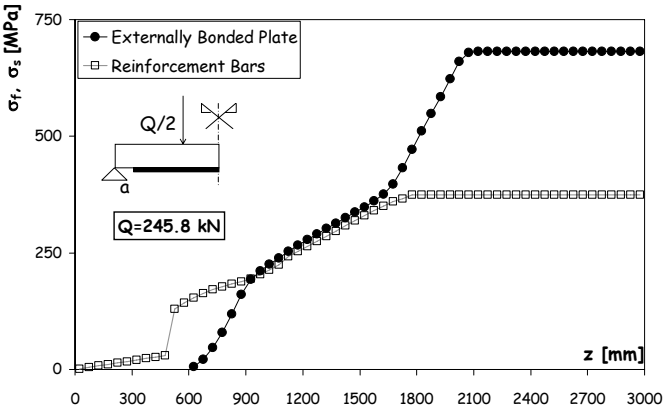

b) axial strains in steel and FRP at (end) debonding;

Figure 12. Debonding phenomenon for partial strengthening.

In this second case, end-debonding failure occurs before of intermediate debonding because the ultimate slip value is achieved at FRP cut-off section under an ultimate load value slightly lesser than the one obtained for complete strengthening.

Finally, although in the present paper the main emphasis is placed upon intermediate debonding, Figure 10 and Figure 12, among the other ones, show how the proposed procedure can simulate both end and intermediate interface debonding failure.

The above results pointed out that there is a direct relationship between the yielding phenomenon and the occurrence of premature failure due to intermediate debonding. This relationship can be clearly pointed out by considering a parametric variation of the rebar yield stress f_{sy} (and strain ε_{sy}) for the first beam characterized by the complete FRP strengthening. Yielding stress values f_{sy} spanning from 215 to 700 MPa (and ε_{sy} correspondingly between 0.00102 and 0.00333) have been considered along with three possible values for the concrete compressive strength f_{ck} (15 to 25 MPa) which affects the value of fracture energy of the adhesive interface. Figure 13 reports the results of this parametric investigation pointing out the direct relationship between the maximum axial strain $\varepsilon_{f,db}$ developed in FRP at debonding (obtained as the maximum value of the interface slip achieve the ultimate value s_u assumed for the interface relationship) and the value of the axial strain ε_{sy} at yielding. Three series of data have been represented for considering the effect of fracture energy values upon the occurrence of intermediate debonding phenomenon. Although the values attained by $\varepsilon_{f,db}$ in correspondence of the greater values of G_f are always greater than the ones achieved for the lesser ones, the mentioned figure points out that $\varepsilon_{f,db}$ is not as greater as G_f (or its square root, as currently assumed even by the most up-to-date codes of standards), but is hugely affected by the value of ε_{sy}.

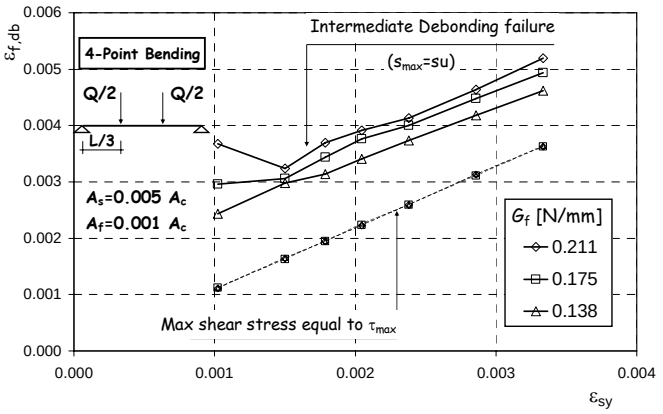

Figure 13. Maximum FRP axial strain at debonding versus rebar yielding strain.

Moreover, the same figure also reports the values of axial strains developed in FRP when the maximum value of the shear stress $\tau=\tau_{max}$ is achieved at

the FRP-to-concrete interface; whatever the fracture energy be such a value is always strictly related to the occurrence of yielding in steel rebars: consequently, the value of such an axial strain is often close to ε_{sy}. This result points out the need to account for the complete bi-linear law in order to carefully simulate the behavior of the adhesive interface and evaluate a consistent value for $\varepsilon_{f,db}$ (as already shown by Figure 11). The present model (despite the other mentioned ones available in the scientific literature), based on a secant treatment of a closed-form solution for the flexibility and stiffness matrix of the strengthened beam, can easily follow the softening branch of the interface relationship by progressively relaxing the value of the interface stiffening without experiencing problems of localization which possibly affect the performance of finite elements when used for simulating softening behavior.

The distance shown in Figure 13 between the values of $\varepsilon_{f,db}$ and the corresponding axial strains at rebar yielding basically depends upon a series of parameters among which the rebar area; Figure 13 deals with a case of relatively small steel reinforcement area, while Figure 14 shows the possible relationship between the two relevant values achieved by FRP axial strain and the rebar steel area A_s, taken as a percentage of the concrete gross section A_c. The figure shows how the distance between $\varepsilon_{f,db}$ and the corresponding value obtained for $\tau=\tau_{max}$ is as great as the rebar area is small; moreover, for the lower values of A_s, the yielding phenomenon results in a non-relevant increase of interface shear stress (if A_s would be null, no increase occurred at all), and a weaker relationship exists between the two values within this range of A_s.

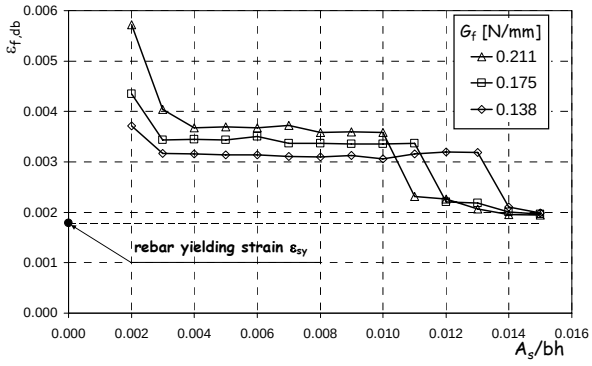

Figure 14. Maximum FRP axial strain at debonding versus rebar area A_s.

Load pattern also affects the debonding phenomenon; Figure 15 compared with Figure 13 shows that greater values are developed for FRP strain at debonding $\varepsilon_{f,db}$ especially for the lower values of rebar strain (and stress) at yielding ε_{sy}. Further differences can be observed in the case of distributed load pattern where intermediate debonding phenomenon usually occurs in a section not close to the maximum bending moment, as usually does under point load condition. This aspect, already mentioned in Thomsen et Al. (2004), is deeply examined in Faella et Al. (2007).

Finally, the role of fracture energy G_f as a parameter which affects both end and intermediate debonding is pointed out in Figure 16 which compares the values of maximum FRP strain at debonding $\varepsilon_{f,db}$ developed throughout the adhesive interface for the two cases mentioned at the beginning of the present section.

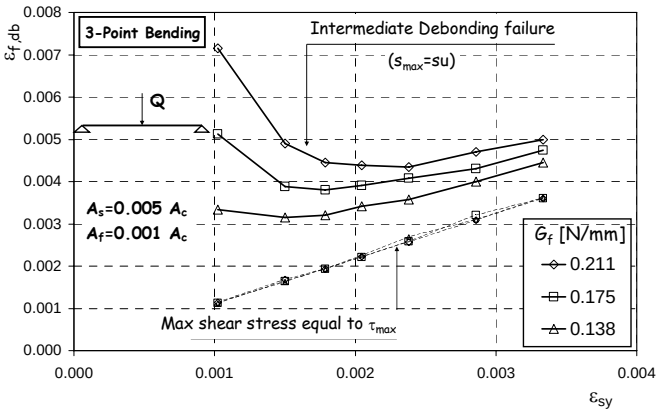

Figure 15. Maximum FRP axial strain at debonding versus rebar yielding strain – Three-Point Bending.

In the case of complete strengthening, intermediate debonding crisis always occurs while different failure modes can be observed for the case of end debonding as the value of G_f increases. For the lower value of G_f, end debonding prematurely occurs in the RC beam partially strengthened by FRP. Failure of the same beam is less and less premature as G_f increase; increase in G_f (almost) directly result in a corresponding growth of strength against end debonding, while yielding in steel rebars occurs resulting in intermediate failure even for the case of incomplete strengthening for the greater value considered of fracture energy G_f.

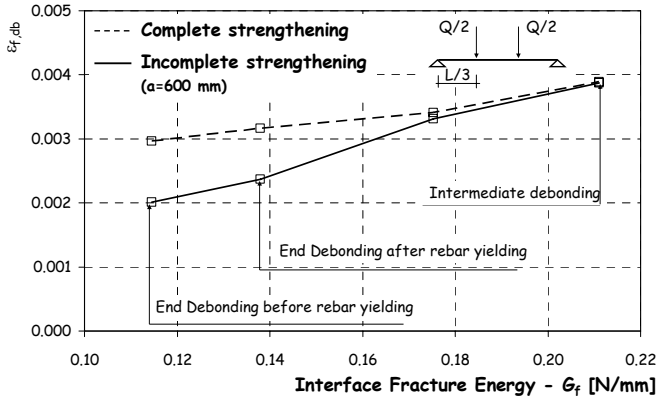

Figure 16. Failure mode versus Fracture energy G_f.

In other words, Figure 16 confirms that fracture energy G_f plays a quite different role in controlling end and intermediate debonding; indeed, strength against the former failure mode is directly enhanced as G_f increases, as assumed by both theoretical find-

ings (see Taljsten, 1997) and the current code of practice. On the contrary, Intermediate debonding, is directly controlled by rebar steel yielding and fracture energy can only partially affect the value of either the load Q achieved at debonding or the maximum strain $\varepsilon_{f,db}$ developed in FRP.

5 CONCLUSIONS

A numerical model has been formulated for simulating the flexural behavior of RC beams strengthened by means of externally bonded FRP systems. Validation of the presented model has been briefly outlined with respect to the results of an experimental test carried out on a beam under four-point bending which failed for intermediate debonding.

Behavioral observations have been drawn with reference to a simply supported beam with the main aim of pointing out the key differences between end and intermediate debonding. Accounting for the softening branch of the shear-stress-interface-slip relationship is of key importance for emphasizing the relative ductility which can be observed in the cases of intermediate debonding failure especially when quantifying FRP maximum strain rather than the maximum force at debonding is of main concern.

Finally, the role of fracture energy G_f has been investigated with respect to both end and intermediate debonding, pointing out its quite diverse influence in controlling these two kinds of premature failure. General remarks should be deduced by these results about the possible enhancement of the simplified formulae available within the scientific literature for evaluating the maximum FRP strain at debonding $\varepsilon_{f,db}$, whose dependence by key parameters like the steel yielding strain ε_{sy} and the amount of rebar are currently neglected. Moreover, the key role played by ε_{sy} and emphasized by the results of the proposed analyses point out the importance of the initial state of stress in the real RC beams which are usually pre-loaded and pre-cracked due to the presence of the self-weights.

ACKNOWLEDGEMENTS

The present paper deals with the subject of concern of the Line 8 – Task 2 of the DPC/ReLUIS Research Project that partially granted the research.

REFERENCES

ACI Committee 440.2 R-02 (2002): Guide for the Design and Construction of Externally Bonded FRP Systems for Strengthening Concrete Structures, Revised 28;

Chen J.F., Teng J.G. (2001): Anchorage Strength Models for FRP and Plates Bonded to Concrete, ASCE Journal of Structural Engineering, vol. 127, No. 7, July, 784-791;

CNR DT 200 (2004): Instructions for Design, Execution and Control of Strengthening Interventions by Means of Fibre-Reinforced Composites (in Italian), Italian National Research Council;

Faella C., Martinelli E., Nigro E., (2002): Steel and concrete composite beams with flexible shear connection: "exact" analytical expression of the stiffness matrix and applications, Computer & Structures, Vol. 80/11, pp. 1001-1109.

Faella C., Martinelli E., Nigro E., (2003): Interface Behaviour in FRP Plates Bonded to Concrete: Experimental Tests and Theoretical Analyses, Proceedings of the 2003 ECI Conference on Advanced Materials for Construction of Bridges, Buildings, and Other Structures III, Davos (Switzerland), 7-12 September;

Faella C., Martinelli E., Nigro E. (2006a): Formulation and Validation of a Theoretical Model for Intermediate Debonding in FRP Strengthened RC Beams, Proceedings of the 2nd fib World Conference, Naples (Italy), June 5-8, 2006, Paper 0735;

Faella C., Martinelli E., Nigro E. (2006b): Intermediate Debonding in FRP Strengthened RC Beams: A Parametric Analysis, Proceedings of the 2nd fib World Conference, Naples (Italy), June 5-8, 2006, Paper 0993.

Faella C., Martinelli E., Nigro E. (2007): Intermediate Debonding of RC Beams Strengthened in Bending by FRP: a Theoretical Model and a Simplified Design Approach, Accepted for publication in the Proceedings of the 8th Sym. FRCRCS, Paper 192, Patras (Greece), July 16-18, 2007;

Gao B, Kim J.K., Leung C. K. Y. (2004): Experimental study on RC beams with FRP strips bonded with rubber modified resins, Composites Science and Technology, 64 (2004) 2557–2564

Holzenkaempfer (1994), Ingenieurmodelle des verbundes geklebter bewehrung fur betonbauteile, Dissertation, TU Braunschweig (in German);

JSCE (2001): Recommendations for upgrading of concrete structures with use of continuous fiber sheets, Concrete Engineering Series 41;

Malek A. M., Saadatmanesh H., Ehsani M. R. (1998), Prediction of failure load of R/C beams strengthened with FRP plate due to stress concentration at the plate end, ACI Structural Journal, Vol. 95, No. 2, , 142-152;

Newmark N. M., Siess C.P., Viest I.M. (1951): Tests and Analysis of Composite Beams with Incomplete Interaction, Proc. Soc. Exp. Stress Analysis, 9, 1951, 75-92;

Roberts T. M. (1988): Approximate analysis of shear and normal stress concentrations in the adhesive layer of plated RC beams, The Structural Engineer, Vol. 66, No. 5, 85-94;

Saenz, L.P. (1964): Discussion of Equation for the Stress-Strain Curve of Concrete by Desayi and Krishman, ACI Journal Vol. 61, pp. 1229-1235;

Taljsten B. (1997), Strengthening of Beams by plate bonding, Journal of Materials in Civil Engineering, ASCE, 9 (4), 206-212;

Task Group 9.3 (2001), Externally Bonded FRP Reinforcement for RC Structures, Technical Report Bulletin 14, fib-CEB-FIP;

Teng J.G., Chen J.F., Smith S.T., Lam L. (2002): FRP-strengthened RC Structures, J. Wiley & Sons, GB;

Thomsen H., Spacone E., Limkatanyu S., Camata G. (2004): Failure Mode analysis of Reinforced Concrete Beams Strengthened in Flexure with Externally Bonded Fiber-Reinforced Polymers, ASCE Journal of Composites for Constructions, vol. 8, n. 2, April, pp. 123-131.